Unique Uptake of Acid-Prepared Mesoporous Spheres by Lung Epithelial and Mesothelioma Cells

Steven R. Blumen*, Kai Cheng*, Maria E. Ramos-Nino, Douglas J. Taatjes, Daniel J. Weiss, Christopher C. Landry, and Brooke T. Mossman

Department of Pathology and Department of Medicine, University of Vermont College of Medicine; and Department of Chemistry, University of Vermont, Burlington, Vermont

Lung cancers, malignant mesotheliomas (MM), and fibrosis are devastating diseases with limited treatment strategies, in part due to poorly-effective drug delivery to affected areas of lung. We hypothesized that acid-prepared mesoporous spheres (APMS) (1–2 μm diameter, 40 Å pore size) might be effective vehicles for pulmonary chemotherapeutic drug delivery. To assess this, APMS, chemically modified with different surface molecules (lipid, a linker having a terminal amine group, a thiol group, or tetraethylene glycol [TEG]), were evaluated for uptake and possible cytotoxic effects after *in vitro* administration to murine alveolar epithelial Type II (C10) and human mesothelioma (MM) cells and after intrapleural or intranasal administration to C57Bl/6 mice. APMS coated with TEG (APMS-TEG) were most efficiently taken up by C10 and MM cells. The mechanism of cell uptake was rapid, actin-dependent, and did not involve clathrin- or caveolae-mediated mechanisms nor fusion of membrane-bound APMS with lysosomes. When injected intrapleurally in mice, APMS-TEG were taken up by both CD45-positive and -negative cells of the diaphragm, lung, and spleen, whereas APMS administered by the intranasal route were predominantly in lung epithelial cells and alveolar macrophages. After intrapleural or intranasal administration, APMS were nonimmunogenic and nontoxic as evaluated by differential cell counts and lactate dehydrogenase levels in bronchoalveolar and pleural lavage fluids. In the treatment of lung and pleural diseases, APMS-TEG may be useful tools to deliver chemotherapeutic drugs or molecular constructs.

Keywords: uptake; particles; nanoparticles; lung cancer; mesothelioma

Nanoparticles, defined as particles of less than 0.1 μm in diameter, have been proposed in the treatment of a number of diseases (1–3). However, due to their small size, many of these particles can enter cell organelles and disrupt normal cell functions (2, 3). In addition, various particles in the nano-scale range also have systemic effects as they are dispersed by the systemic circulation, and may also cross the blood–brain barrier (1–3). Thus, there are general concerns regarding potential toxic and systemic effects of nanoparticles after administration. To circumvent these problems, we developed a novel fine particle for the delivery of various drugs and other molecules. We hypothesized that targeted drug delivery of respirable fine particles (defined as 0.1–2.5 μm diameter) (4) intranasally or intrapleurally would be nontoxic and beneficial in a number of airway and pleural diseases.

(*Received in original form August 28, 2006 and in final form October 5, 2006*)

* These authors contributed equally to the research described in this paper.

This work was supported by P01HL67004 from NHLBI (B.T.M.) and T32ES0071 from NIEHS (S.R.B.)

Correspondence and requests for reprints should be addressed to Dr. Brooke Mossman, University of Vermont College of Medicine, Department of Pathology, 89 Beaumont Avenue, HSRF 218, Burlington, VT 05405. E-mail: Brooke.Mossman@uvm.edu

Am J Respir Cell Mol Biol Vol 36. pp 333–342, 2007
Originally Published in Press as DOI: 10.1165/rcmb.2006-0319OC on October 12, 2006
Internet address: www.atsjournals.org

CLINICAL RELEVANCE

The research presented introduces a novel method (APMS) of delivering drugs or constructs to cells in the treatment of lung and pleural diseases. Acid-prepared mesoporous spheres enter cells via a rapid, actin-dependent mechanism, which is not membrane-bound.

Acid-prepared mesoporous spheres (APMS) are amorphous silica-based particles created synthetically (5–7). Unlike crystalline silica, amorphous silica is not associated with the development of lung disease and is nontoxic after administration via a number of routes *in vivo* or *in vitro* (8). Importantly, the APMS contain pores of various size dimensions that can allow them to be loaded with therapeutic drugs and other cargo. Both the diameter of the APMS and the pore size can be modified independently to deliver "cargo" of different solubilities and molecular weights (9).

Studies here were undertaken to characterize the efficiency of uptake of APMS by lung epithelial and malignant mesothelioma (MM) cells *in vitro*. A series of surface modifications were first explored to increase efficiency of APMS uptake by cells and to elucidate possible mechanisms of cell internalization of APMS. There is a large body of literature indicating the use of pegylation of proteins, dendrimers, aptamers, polymers, anticancer drugs, and immunoliposomes to create "stealth particles" that can evade uptake by immune cells and enhance the duration of particle persistence *in vivo* (10–22). Thus, in our experiments, APMS were synthesized and coated with different molecules, including tetraethylene glycol (TEG), a short-chain polyethylene glycol. Since APMS-TEG were most avidly taken up by lung epithelial (C10) and human MM cells and were nontoxic to cells at high concentrations, the mechanisms of uptake of APMS-TEG were characterized further. Unlike ultrafine or nanoparticles, APMS were not associated with the endoplasmic reticulum, mitochondria, or endocytotic vesicles. In contrast to pathogenic particulates such as asbestos or silica, cell uptake of APMS-TEG did not involve encapsulation of particles by membranes into phagosomes nor their merging with lysosomes. Their ability to circumvent cellular digestion is a unique feature of APMS-TEG that should permit their delivery of "cargo" intracellularly without potential degradation after inhalation or intrapleural administration.

MATERIALS AND METHODS

Cells and Reagents

Murine alveolar epithelial Type II cells (C10) (23) were maintained in CMRL 1066 (P139-500; Biosource, Rockville, MD) supplemented with 10% fetal bovine serum (FBS) (35-010-CV; Mediatech, Herndon, VA), 2 mM L-glutamine (25030–156; GIBCO, Invitrogen, Carlsbad, CA), and

penicillin-streptomycin (50 U/ml penicillin G, 50 μg/ml streptomycin sulfate) (15140-122; GIBCO). Human MM cells kindly obtained from Dr. Luciano Mutti (Maugeri Foundation, Pavia, Italy) were maintained in DMEM/F12 50/50 medium (10-092-CV; Mediatech) supplemented with 10% FBS, 0.1 μg/ml hydrocortisone (H-0135; Sigma, St. Louis, MO), 2.5 μg/ml insulin, 2.5 μg/ml transferrin, 2.5 ng/ml sodium selenite (I-1884; Sigma) and penicillin-streptomycin (50 U/ml penicillin G, 50 μg/ml streptomycin sulfate) (15140–122, GIBCO). Unless otherwise specified, reagents were purchased from Sigma.

Synthesis of APMS

Cetyltrimethylammonium bromide (CTAB) (4.9 mM) was suspended in 53.75 ml of an ethanol and distilled water mixture (at a 1:2.8 ratio). Concentrated hydrochloric acid (HCl, 3.7 ml) was added, and the mixture stirred until fully dissolved. Tetraethoxysilane (TEOS, 4.29 ml) was then added with stirring for 5 min, followed by addition of 4.67 ml of 0.5 M sodium fluoride (NaF, in water), the mixture heated at 373 K for 40 min, and the resulting white precipitate captured by filtration, washed 1× with distilled H_2O, and air dried. The synthesized APMS were placed under high vacuum to remove the remaining moisture.

Synthesis of APMS-NHMe, APMS-NH_2, and APMS-SH

To modify their surface, APMS were reacted with an organosilane containing the target functionality. As an example, to synthesize secondary amine-terminated particles, APMS (1 g) and *N*-methyl-propylaminetrimethoxysilane (2 mM) were added to hexane (20 ml), and the mixture was heated at 333 K for 2 h. After cooling to room temperature, the solid was filtered, washed with hexane and ethanol, and dried at 373 K in air. To remove the surfactant (CTAB), 1 g of amine-modified APMS with *N*-methyl-propylamine functionality (APMS-NHMe) was refluxed twice for 6 h in ethanol followed by extensive washes with ethanol. The resulting APMS-NHMe then was dried under high vacuum. To prepare APMS-NH_2 and APMS-SH, identical procedures were followed except that the amine was replaced with aminopropyltrimethoxysilane and mercaptopropyltrimethoxysilane, respectively.

Synthesis of APMS-Lipid and Fluorescently-Labeled APMS

To synthesize APMS with a lipid-modified surface, APMS-NH_2 (0.300 g) was suspended in a solution of oleic acid (0.349 g) in *N*,*N*′-dimethylformamide. Standard peptide bond-forming methodology (24) was used to attach the acid to the surface, and after stirring at room temperature for 12 h, the resulting material was captured by filtration, washed and dried in air, and stored under vacuum. APMS could easily be covalently labeled with appropriate fluorescent dyes, such as Alexa-488 succinimide ester (Molecular Probes, Eugene, OR), by forming peptide bonds.

Synthesis of APMS-TEG

A half gram of APMS-NHMe was suspended in 10 ml of anhydrous ethanol containing mono-tosylated tetraethylene glycol (Ts-TEG) (0.5 mM). The mixture was then refluxed for 6 h. The resulting APMS-TEG was captured by filtration, washed with ethanol, and dried in air. The APMS-TEG were placed under high vacuum to remove the remaining solvent.

Synthesis of APMS-TEG Preloaded with Plasmid

Two milligrams of APMS-TEG modified with Alexa-633 was combined with 1 ml of 0.2 M $MgCl_2$, sonicated for 10 min, and incubated at room temperature overnight. The supernatant was decanted, and APMS were dried in a vacuum. One milligram of the APMS was then combined with 0.2 ml PBS (pH 7.2) containing 10 μg of the plasmid, pCMV-DsRed-Express (Clontech Laboratories, Inc., Mountain View, CA), and sonicated for 30 min. Samples were then centrifuged, APMS were washed 2× in PBS, and samples were dried in a vacuum.

Treatment of Cells with APMS

Cells were plated and grown to 70–80% confluence at 37°C in complete medium. Medium was aspirated and replaced with maintenance medium containing 0.5% FBS, and incubated for 24 h. APMS were then resuspended in medium containing 0.5% FBS serum at a concentration of $\sim 6 \times 10^7$ APMS per 100 μl, mixed well, and sonicated 5× for 2 s, to disperse any clumps. Fifty microliters were then added to cells at a final density of $7.5 \times 10^6/cm^2$ surface area dish (i.e., $\sim$ 185 particles/cell).

Lactate Dehydrogenase Measurement for Measurement of Cell Damage *In Vitro*

Cells were treated with APMS for various amounts of time, and lytic cell damage was measured by determining levels of lactate dehydrogenase (LDH) released into the medium using Cytotox 96 kit (Promega, Madison, WI), as per manufacturer's recommendations.

Sample Preparation for Scanning Electron Microscopy and Transmission Electron Microscopy

Cells were grown on Thermanox plastic coverslips (Nalge Nunc International, Naperville, IL) in 12-well plates as described above, and treated with APMS for various amounts of time. Coverslips were washed 2× for 5 min with 0.1 M Millonig's phosphate buffer (pH 7.2), then fixed in 1:1 H_2O dilution of Karnovsky's fixative (2.5% glutaraldehyde, 1% paraformaldehyde) at 4°C for 45 min. Samples were then washed with Millonig's phosphate buffer (pH 7.2), and post-fixed in osmium tetroxide (OsO_4) at 4°C for 30–45 min. Samples were then dehydrated in graded ethanols, from 35% to 100%.

Scanning Electron Microscopy

Samples prepared as described above were critical point dried using liquid CO_2 as the transition fluid in a Samdri PVT-3B critical point dryer (Tousimis Research Corporation, Rockville, MD). Specimens were mounted on aluminum specimen stubs using conductive graphite paint and allowed to dry, and were sputter-coated for 4–5 min with gold and palladium in a Polaron sputter coater (Model 5100; Quorum Technologies, Guelph, ON, Canada). Specimens were then examined with a JSM 6060 scanning electron microscope (JEOL USA, Inc., Peabody, MA).

Transmission Electron Microscopy and Elemental Analysis

Samples were prepared as described above and were infiltrated with Spurr's resin according to the following schedule: (100% ethanol:Spurr's resin) 3:1 for 30 min; 1:1 for 30 min; 1:3 for 30 min; and 100% Spurr's resin for 30 min. Flat embedding molds were filled with Spurr's resin, and coverslips were placed onto the surface of the resin, cell side down. Resin was then polymerized overnight at 70°C. Polymerized blocks were plunged into liquid nitrogen to facilitate peeling of the coverslips from the resin block, and the resin blocks were cut into pieces and remounted onto blank blocks for sectioning.

Semi-thin sections (1 μm) were cut using glass knives on a Reichert Ultracut microtome, stained with methylene blue–azure II, and evaluated for areas of cells. Ultra-thin sections (60–80 nm) were cut with a diamond knife, retrieved onto 150 mesh copper grids, contrasted with uranyl acetate (2% in 50% ethanol) and lead citrate, and examined with a JEM 1210 transmission electron microscope (JEOL USA, Inc.) operating at 60 kV.

Energy-Dispersive Spectroscopy

Grids from transmission electron microscopy (TEM) samples were analyzed, or portions of coverslips processed for scanning electron microscopy (SEM) were cut after critical point drying and fixed onto copper bulk holders with conductive tape. They were sputter-coated with gold and palladium as described above. Cells were imaged, and energy-dispersive spectroscopy (EDS) was performed on samples by STEM with a JEM 1210 transmission electron microscope (JEOL USA, Inc.), equipped with an energy-dispersive X-ray spectrometer and IMIX software, version 7 (hardware and software from Princeton Gamma-Tech, Princeton, NJ). Accelerating voltage on the JEOL was 20 kV. A spot analysis of APMS was performed with the IMIX collecting at 0–20 keV.

Confocal Scanning Laser Microscopy

Cells were grown on glass-bottom culture dishes (P35G-1.5-14-3; MatTek Corporation, Ashland, MA) and treated with APMS as described above. Cells were subsequently incubated with the nucleic acid dye, Hoechst 33342 (H3570; Molecular Probes, Invitrogen), for 15 min.

Medium was then removed and replaced with 1 ml ice-cold Ca^{++} and Mg^{++}-free Hank's Balanced Salt Solution without Phenol Red, containing 5 μg/ml membrane dye FM4-64 (T3166; Molecular Probes, Invitrogen). Samples were kept on ice and immediately viewed on a Zeiss LSM 510 META confocal scanning laser microscope (Carl Zeiss Microimaging, Thornwood, NY).

Determination of Mechanisms of APMS Uptake by Flow Cytometry

Cells were exposed for 30 min to chemical inhibitors of specific uptake mechanisms: chlorpromazine (5 μg/ml), cytochalasin D (1 μM), or filipin (6.25 μg/ml)—that is, at effective concentrations as reported in the literature (25–29)—or incubated at 4°C for 30 min before addition of APMS for various amounts of time. Hoechst 33342 nucleic acid dye (16.2 μM) (Molecular Probes, Invitrogen) was added 15 min before harvesting cells. Cells were washed once in PBS and removed from dishes using Accutase cell detachment solution (Innovative Cell Technologies, Inc., San Diego, CA), pelleted by centrifugation, resuspended in calcium and magnesium-free PBS, and kept on ice until analyzed. Samples were analyzed using a BD LSRII flow cytometer (BD Biosciences, San Jose, CA) equipped with a Sapphire 488 (Coherent, Santa Clara, CA) laser that emits at 488 nm to excite the Alexa 488 dye, and a solid state Xcite (Lightwave) that emits at 355 nm to excite the Hoechst 333342 nucleic acid dye (Molecular Probes, Invitrogen). Data analysis was performed at the time of acquisition using Flow Jo (Tree Star, Inc., Ashland, OR). This software package is an experiment-based flow cytometry data analysis package designed for multicolor research.

To verify that the gating used in determining cell populations was accurate, FACS analysis was performed on different populations. Populations of cells/APMS were selected based on their locations on histograms, and were sorted, collected, and mounted on glass slides using cytocentrifugation. Cell sorting was accomplished using a BD FACSARIA (BD Biosciences) equipped with the following lasers: a Sapphire 488 (Coherent) that emits at 488 nm to excite the Alexa 488 dye, and an IFlex 2000-P1-405 (Point Source, Southampton, UK) that emits at 407 nm to excite the Hoechst 33342 nucleic acid dye. The fluorescent signals from Alexa 488 were detected using 530/30 BP and 505 LP filters. Hoechst staining was detected using 440/40 BP filter. Identification and quantification of populations on cytospins were performed manually with phase contrast and fluorescence microscopy using an Olympus BX50 microscope (Olympus America, Lake Success, NY).

Delivery of Functional Plasmid Using APMS

C10 cells were grown on glass coverslips for 24 h. APMS conjugated with the DNA plasmid, pCMV-DsRed-Express (Clontech Laboratories) were then added to cells at 37°C for 24 h. Cells were washed 3× with PBS, fixed in 4% paraformaldehyde, washed 3× in PBS, and incubated with 1 μM SYTOX Green (Molecular Probes, Invitrogen) for 5 min at room temperature. Coverslips were washed 3× in PBS, mounted on glass slides, and viewed using CSLM.

Intrapleural Injection of APMS

APMS were suspended in PBS at a concentration of $\sim 4 \times 10^7$ APMS per 100 μl PBS. Samples were then mixed well and sonicated 5 × 2 s to obtain an even suspension. C57Bl/6 Mice were anaesthetized temporarily using isoflurane, and APMS were then injected into the pleural cavity between the third and fourth right side intercostals. The needle was inserted under the ribcage so as not to puncture the lung, and 100 μl of the APMS/PBS suspension was injected. Sham control mice received 100 μl of PBS alone. Mice were observed until fully recovered and for any adverse effects, and were killed after 3 or 7 d by intraperitoneal injection of sodium pentobarbital.

Intranasal Instillation of APMS

APMS were suspended in PBS at a concentration of $\sim 4 \times 10^7$ APMS per 50 μl PBS. Samples were mixed well and sonicated 5 × 2 s to obtain an even suspension. Mice were then anaesthetized temporarily by exposure to isoflurane in a Bell jar, and APMS were instilled by placing small drops on the nostrils of the mice and allowing them to inhale 50 μl of APMS/PBS solution. Repeated short exposures to isoflurane were necessary to complete the instillation. Mice were observed until fully recovered and for any adverse effects. After intranasal administration, mice were allowed to recover for 6 or 24 h, after which they were killed as described above.

Tissue Processing

The effects and fate of APMS *in vivo* were determined by examining lungs, rib cage, diaphragm, spleen, and heart. Tissues were removed surgically and either placed in Tissue-Tek O.C.T. compound (Sakura Finetek USA, Torrance, CA) and snap-frozen, or fixed in 4% paraformaldehyde and paraffin embedded.

Detection of APMS and Inflammatory Mediators in Pleural Lavage Fluid or Bronchoalveolar Lavage Fluid

Recovery of pleural lavage fluid. Pleural lavage fluid (PLF) was obtained after opening of the peritoneal cavity and injecting 2.0–3.0 ml of PBS through the diaphragm into the chest cavity, gently massaging the chest and then recovering the fluid, which was measured for volume.

Recovery of bronchoalveolar lavage fluid. A cannula attached to a syringe was inserted into the trachea of animals, 1 ml of PBS instilled into the trachea, and the lungs were gently massaged. The fluid was then recovered and measured.

LDH and protein measurement. Tissue damage was measured by determining levels of LDH in fresh PLF and BALF samples using Cytotox 96 kit (Promega), and protein levels in PLF and BALF were determined using a Bio-Rad Protein Assay Kit (Bio-Rad Laboratories, Inc., Hercules, CA).

Cytospins and cell differentials. Cytospins from PLF and BALF were made in duplicate by resuspending 50,000 cells in 450 μl of medium containing 7–10% FBS and cytocentrifugation for 10 min at 600 rpm. Slides were then air-dried and fixed for 5 min in 100% methanol, followed by Wright-Giemsa staining using HEMA 3 kit (Fisher Scientific, Kalamazoo, MI) as per the manufacturer's recommendations to allow identification of cell types.

CSLM and CD45 staining for determination of APMS location in vivo: Tissue sections were obtained from frozen tissues, fixed in 4% paraformaldehyde, and either viewed via CSLM as described above, or stained for the leukocyte common antigen, CD45. Briefly, paraformaldehyde-fixed sections were rinsed in PBS, blocked for 1 h at room temperature in 5% normal donkey serum, 0.5% bovine serum albumin (BSA) in PBS, then incubated overnight at 4°C in a 1:500 dilution of anti-CD45 antibody (MCD4500; Caltag Laboratories, Burlingame, CA) in 0.5% BSA, 0.1% Triton X-100 in PBS. Slides were then rinsed in PBS and incubated with secondary antibody, donkey anti-rat conjugated to Alexa 488 (Molecular Probes), and counterstained with the nucleic acid dye, TOTO 3 (Molecular Probes, Invitrogen) or DAPI (Molecular Probes, Invitrogen). Samples were rinsed in PBS, coverslips were mounted, and slides were viewed using CSLM.

Statistical Analysis

For *in vitro* experiments, at least three independent experiments were performed (n = 2–4 per experiment). For *in vivo* experiments, results are representative of at least four mice/duplicate experiments. Statistical significance was evaluated by ANOVA using the Student Neuman-Keul's procedure for adjustment of multiple pairwise comparisons between treatment groups or using the nonparametric Kruskal-Wallis and Mann-Whitney tests. Values of $P < 0.05$ were considered statistically significant.

RESULTS

To determine the effect of surface coating on APMS uptake by C10 and MM cells, different molecules were chemically bound to the outer surface of fluorescently-tagged APMS. When APMS were coated with lipid or a chemical linker having a terminal -NH_2 group, few APMS were observed in cells at 24 h (Figures 1A and 1B). However, when APMS were coated with a linker having a terminal -SH group (Figure 1C), increased APMS appeared to be associated with cells. Coating the APMS with TEG resulted in even further uptake by both C10 (Figure 1D) and MM cells (*see below*). To determine whether surface-coated

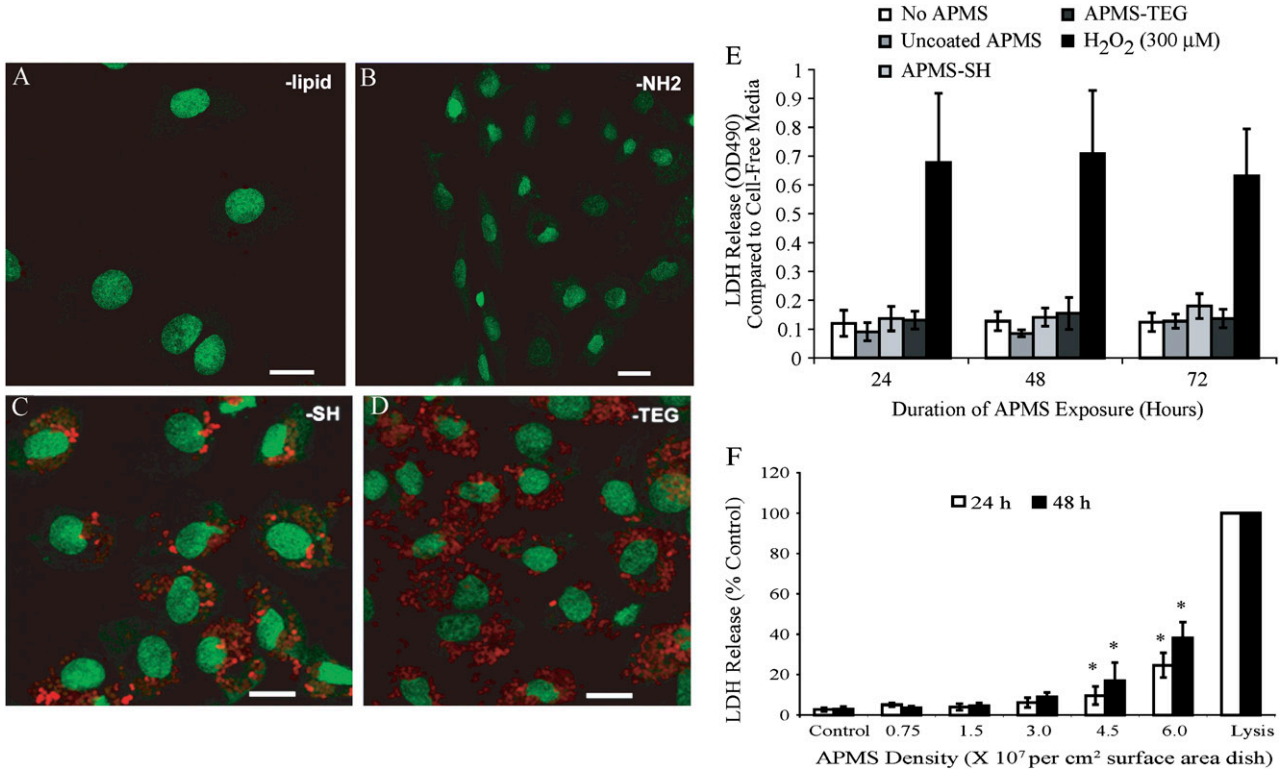

Figure 1. TEG facilitates cell uptake of APMS, which are not cytotoxic to lung epithelial (C10) cells, as measured by release of LDH. APMS were coated with Alexa 568 (*red*) and either lipid (*A*), a linker having a terminal propylamine group (*B*) or a propylthiol group (*C*), or tetraethylene glycol (TEG) (*D*). APMS were added at 7.5×10^6/cm^2 surface area dish. To enhance the contrast, *low-intensity green pixels* (below intensity 30) were colored *black*. Cell nuclei are stained with SYTOX Green. *A, C,* and *D* are at ×400 and *B* is at ×200 magnification (*scale bars* are 20 μm). The effect of surface coatings on APMS-induced cytotoxicity was measured by the LDH assay (*E*), where 300 μM H_2O_2 was used as a positive control for LDH release. *F* shows a dose-response study using APMS coated with TEG in which cell lysis was also measured by the LDH assay. Complete cell lysis was used as a positive control for LDH release. Results are expressed as mean ± SEM from three experiments; *$P < 0.01$ when compared with control group at respective time point.

APMS particles had adverse effects on cells over time, LDH assays were performed after addition of particles for 24, 48, or 72 h These studies showed that densities of APMS up to 0.75×10^7 particles per cm^2 surface area of dish were nontoxic in comparison to 300 μM H_2O_2, a positive control for cell lysis (Figure 1E). To determine the toxicity of various amounts of APMS on MM cells, APMS coated with TEG were incubated with MM cells for 24 or 48 h, and LDH release was measured as an indication of cell damage. As shown in Figure 1F, APMS toxicity was not seen in MM cells until the density of APMS reached 4.5×10^7 particles per cm^2 surface area dish, ~ 6-fold higher amounts than quantities used in studies below.

Since APMS coated with TEG were most effectively taken up by both cell types, the approximate time course of APMS-TEG

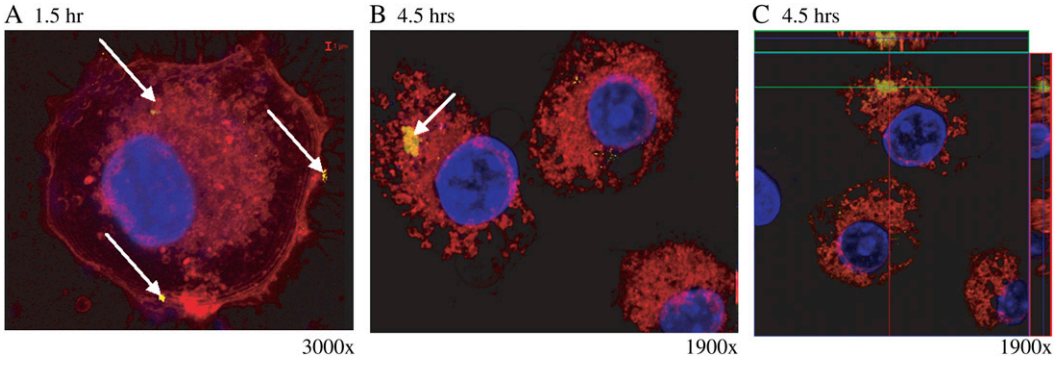

Figure 2. APMS-TEG enter lung epithelial (C10) cells in a time-dependent manner. CSLM images at 1 h (*A*) and 4.5 h (*B* and *C*) after addition of APMS-TEG (0.75×10^7 APMS/cm^2 surface area dish). In *C*, note the cluster of APMS internally that is integrated with membrane-bound organelles (*red*). *Arrows* indicate location of APMS (labeled with Alexa 532, false-colored yellow), and cell nuclei are *blue*. To enhance the contrast in *A*, *low-intensity yellow pixels* (below intensity 30) were colored *black*.

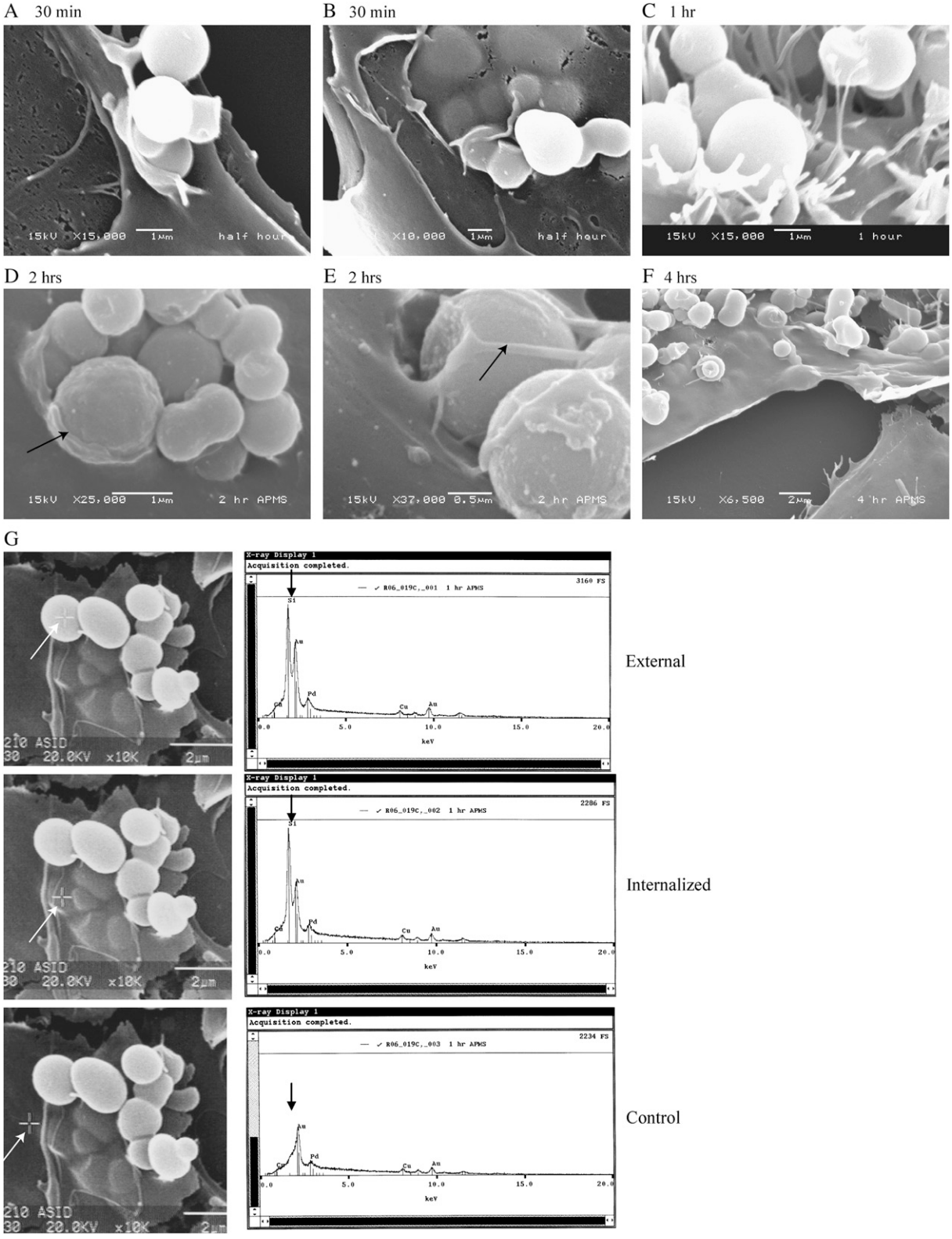

Figure 3. Individual and clusters of APMS-TEG are internalized by MM cells. (*A–F*) are SEM images from a time-course study. Note the *arrows* in *D* and *E* showing partial membrane formation around APMS at the cell surface. *Panels* in *G* show EDS analyses. Crosshairs on SEM images, as indicated by *white arrows*, indicate area probed. The corresponding elemental analysis shows the detection of APMS containing silica in *upper panels*, whereas the *lower panel* shows no silica signal.

uptake by C10 cells was then investigated in living cells using a cell membrane dye (FM4-64) and a nuclear dye (Hoechst 33342) as a counterstain. CSLM allowed the visualization of fluorescent APMS in relationship to cell membranes, as well as determination of whether APMS were inside cells or associated with the cell membrane. To clearly visualize the location of fluorescent APMS in regard to cell membranes, areas of the coverslips were visualized that had relatively few APMS present.

APMS-TEG entered C10 cells within 1 h, although both extracellular and intracellular APMS-TEG were observed at this time (Figure 2A). At 4.5 h, the majority of APMS-TEG were intracellular (Figures 2B and 2C). Figure 2C is an orthogonal view of a CSLM image that allows the visualization of the observed microscopic field additionally in both the x,z- and y,z-planes. Fluorescent APMS (*yellow*) are seen among the membrane-bound cell organelles (*red*), and indicate that APMS are located in the same plane as cell nuclei and that they have therefore entered the cell and are not just associated with the outer cell membrane.

Using SEM, we next determined that APMS-TEG entered MM cells as early as 30 min after their addition to medium. At all time points, most APMS were internalized, but this appeared to be a dynamic process involving interactions of the plasma membrane and microvilli (Figures 3A–3C) with single particles or clusters of APMS-TEG (Figures 3D and 3E). At 4 h, all APMS-TEG were cell-associated (Figure 3F). SEM/EDS confirmed that spheroid particles external to the cell membrane (Figure 3G) or internalized under the plasma membrane (Figure 3G) were APMS (Figure 3G), in contrast to areas without particles that showed no silica peaks (*lower panel*).

To further determine the intracellular location and lack of cytotoxicity of APMS-TEG, MM cells were examined using TEM. At 1 h after incubation of APMS-TEG with MM cells, particles were seen interacting with microvilli and within cells (Figure 4A). Identification of APMS was confirmed using EDS (data not shown). In all sections, intracellular APMS were not enclosed in membrane-bound phagosomes nor phagolysosomes and did not cause toxic alterations in cellular organelles (Figures 4B and 4C).

To understand the mechanisms of uptake of APMS-TEG by MM cells, flow cytometry experiments were performed using fluorescent APMS-TEG covalently linked with Alexa 488. When APMS-TEG were incubated with MM cells at 37°C, an increase in cells containing APMS occurred between 30 min and 4 h (Figure 5). APMS-TEG uptake was significantly inhibited ($P < 0.05$) when cells were maintained at 4°C. We next pre-incubated cells with an inhibitor of caveolae-mediated uptake (filipin), an inhibitor of receptor-mediated endocytosis and clathrin-coated pit-mediated uptake (chlorpromazine), and cytochalasin D, an agent that disrupts actin filaments, for 30 min before addition of APMS-TEG to cells. Compared with the control group at 37°C, no inhibition of particle uptake was observed after pretreatment of MM cells with filipin or chlorpromazine, indicating that APMS-TEG are not taken up by a mechanism involving caveolae or clathrin-coated pits (Figure 5). However, decreased numbers of APMS-containing cells were observed after pretreatment with cytochalasin D, suggesting that APMS-TEG uptake may involve an actin-mediated process.

To determine if APMS could be used as vehicles to deliver functional plasmids, we preloaded the pores of APMS-TEG with a plasmid (pCMV-dsRedExpress) that, if functionally delivered to cells, is transcribed and translated into a protein that fluoresces red. Figure 6 shows a CSLM image of a C10 cell treated with fluorescent APMS-TEG (shown in *blue*, *upper left panel*), and counterstained with a SYTOX Green nucleic acid dye (*lower left panel*). The *upper right panel* is the functional red fluorescent protein, and the *lower right panel* is the merged image. This figure indicates that APMS enter cells and deliver functionally expressed plasmids to cells.

Next, we evaluated the toxicity and possible immunogenicity of APMS-TEG when injected intrapleurally or instilled intranasally in mice. As shown in Figures 7A–7D, injection of APMS-TEG IP did not cause a change in cell populations in PLF or BALF in comparison to sham mice injected with PBS alone. Moreover, injection of APMS-TEG did not alter protein or LDH levels in PLF or BALF (Figures 7E–7H, respectively).

Finally, to determine the fate of APMS-TEG after intrapleural injection or intranasal administration, CSLM was used to locate fluorescently-tagged APMS-TEG in mouse tissues. After intrapleural injection, APMS-TEG were found in rib tissues local to the site of injection, as well as in the diaphragm, spleen, and lung (Figure 8A). APMS-TEG were not found in the heart (data

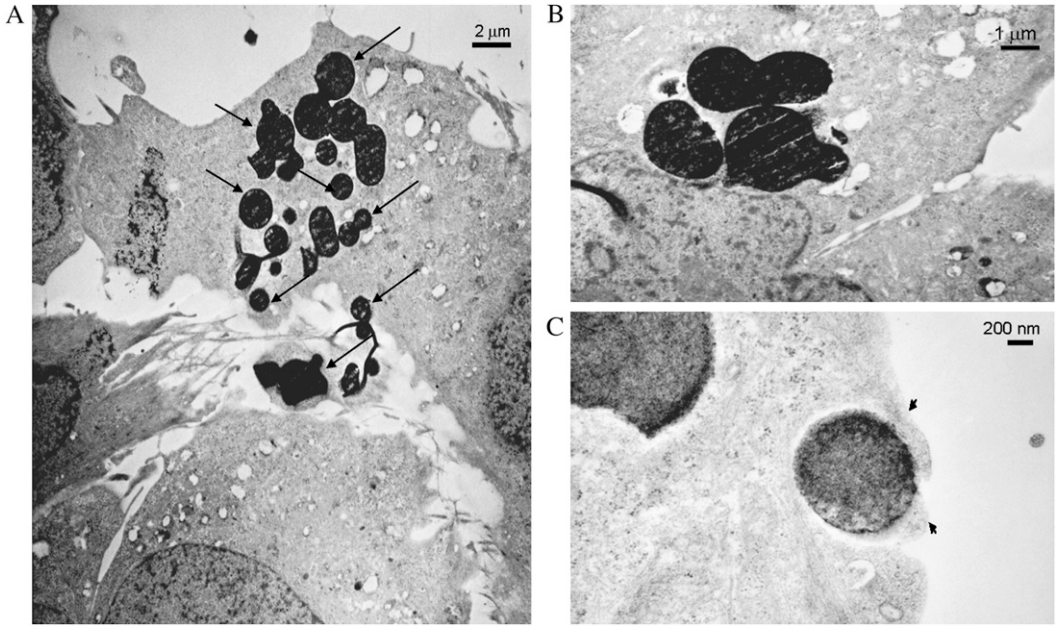

Figure 4. TEM images show APMS-TEG (*arrows*) in the cytosol and intercellularly at 1 h after their addition to MM cells. Note the prominent microvilli interacting with intercellular beads in *A*. *B* shows perinuclear accumulation of APMS-TEG. Non–membrane-bound beads surrounded by cell surface cytoplasm (*arrowheads*) are shown in *C*.

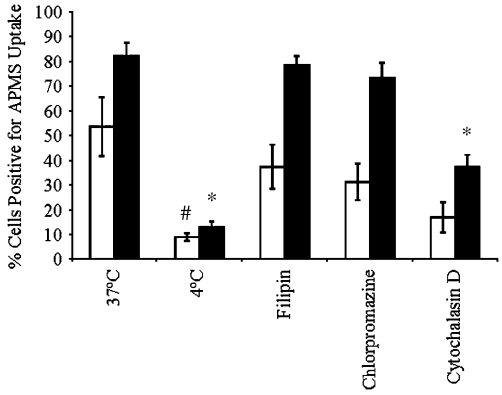

Figure 5. Cell uptake of APMS is an active process not involving clathrin- or caveolae-mediated mechanisms. Flow cytometry after incubation of MM cells at 4°C or 37°C and with or without selective inhibitors (pretreatment for 30 min before addition of APMS) were used to evaluate the percentage of cells positive for APMS uptake at 30 min (*open bars*) or 4 h (*solid bars*). Mean ± SEM from at least three individual experiments. $^{\#}P < 0.05$; $^{*}P < 0.01$ when compared with 37°C group at respective time point.

not shown). In lung tissue, APMS were located occasionally in CD45-positive leukocytes (Figure 8B). After intranasal instillation, APMS-TEG were found primarily in alveolar septa of the lung, where they were observed in both CD45-positive and -negative cells (Figure 8C).

DISCUSSION

Lung cancers and MMs have a poor prognosis, and new treatment approaches are much needed. Combinations of chemotherapeutic agents may be essential (30, 31). Moreover, to avoid systemic toxicity, topical application of agents at sites of early tumor development or surgical debulking of tumors are merited.

APMS are mesoporous nontoxic silica spheres that can be engineered in different size ranges and pore diameters to permit uptake and release of various drugs or DNA/RNA constructs (9). They are extremely versatile, having characteristics that allow the pores and the outer APMS surface to be functionalized differently from each other, providing a wide array of potential uses. In studies here, APMS having different functional groups on the surface were first characterized for their ability to enter lung epithelial and MM cells *in vitro*. APMS coated with TEG, a short chain polyethylene glycol (PEG) molecule, were most readily taken up by both cell types compared with the other coatings. APMS-TEG at 1–2 μm in diameter were able to enter cells efficiently through an active, energy-dependent process. We speculate that the TEG bound to the APMS surface facilitates the interaction of APMS with the plasma membrane, allowing particles to subsequently pass through the membrane individually or in clusters. At later time points, most APMS were observed intracellularly, but some still remained on the cell surface. This may be due to the different amounts of time required for individual APMS particles to settle on or be taken up by cells. Interestingly, APMS-TEG, either individually or in clusters, were taken up efficiently by cells as verified using EDS analysis. Moreover, the presence of APMS-TEG particles intracellularly did not cause obvious cell toxicity over time as

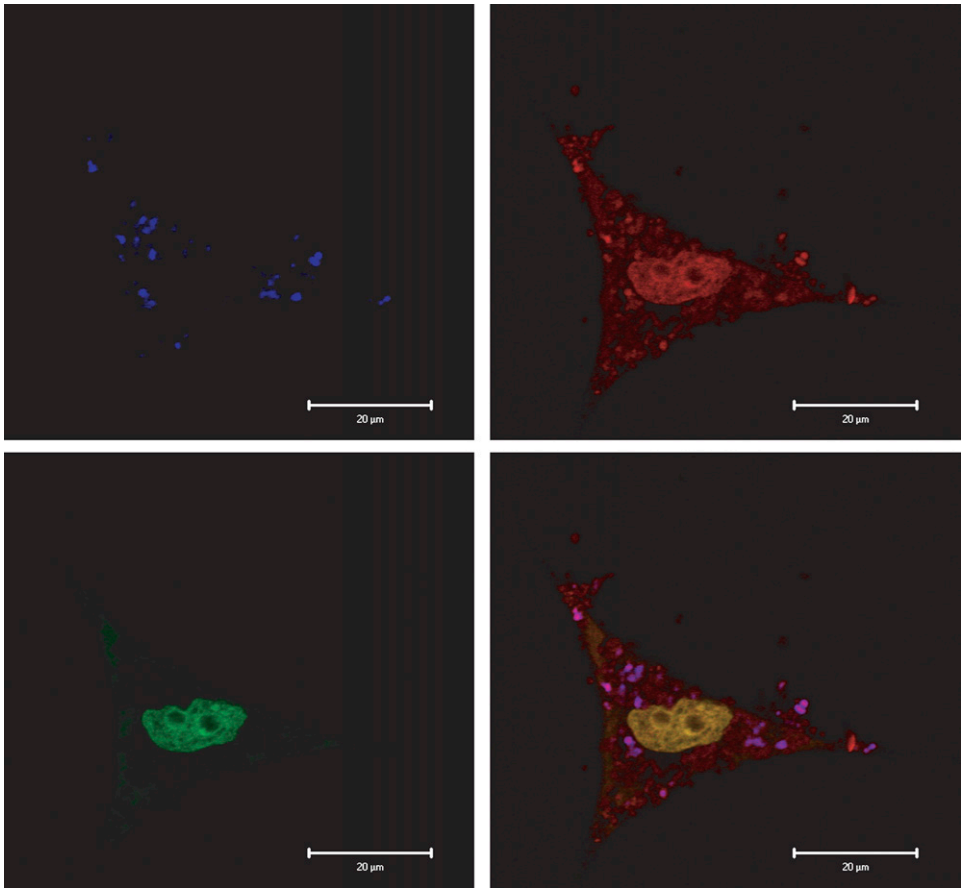

Figure 6. Plasmids delivered by APMS are functionally expressed in lung epithelial (C10) cells. APMS coated with TEG were preloaded with pCMV-DsRed-Express plasmid (Clontech Laboratories, Inc.) and incubated with C10 cells for 24 h CSLM was used to confirm delivery and expression of the plasmid, as seen by the presence of functional red fluorescent protein. The *top left panel* shows fluorescent APMS (Alexa 647, *blue*), the *bottom left panel* shows the cell nucleus in *green* (SYTOX Green), the *top right panel* shows functional expression of the plasmid (*red*), and the *bottom right panel* is the merged image. *Scale bar* = 20 μm.

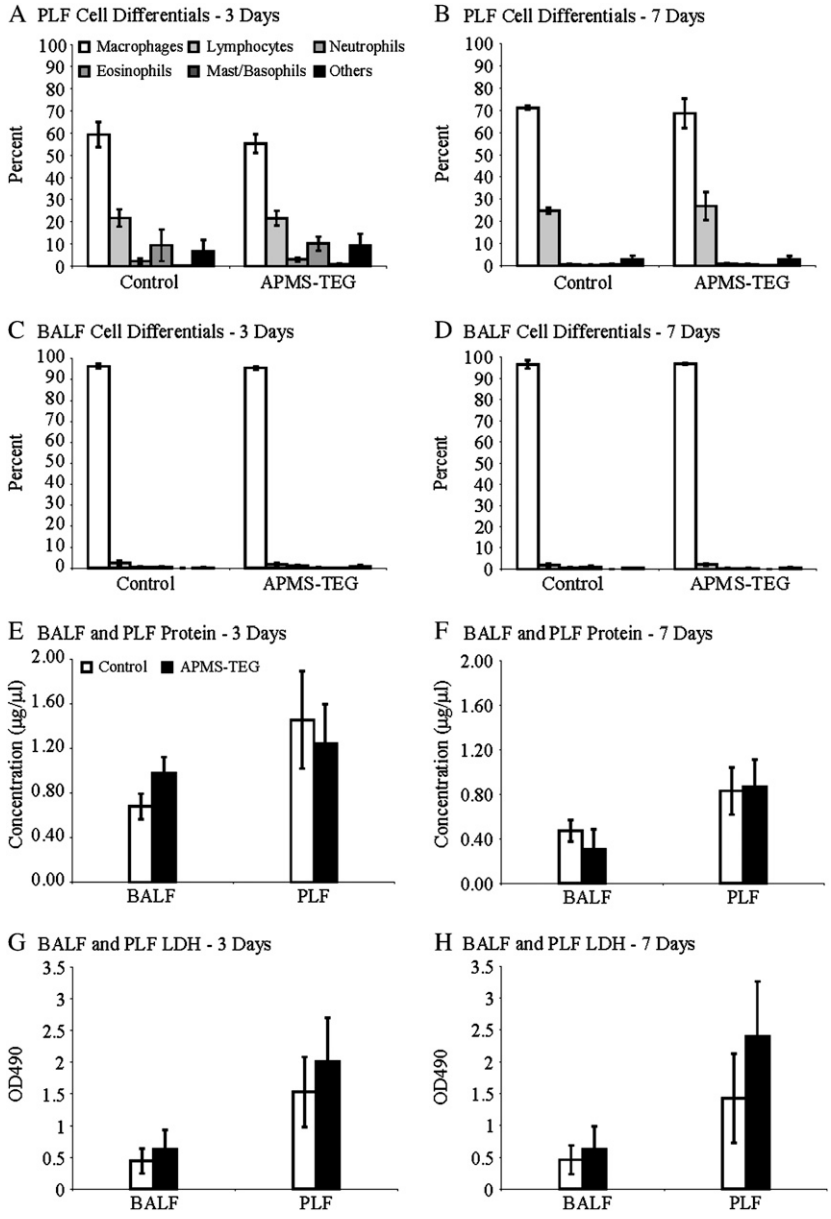

Figure 7. Differential cell counts, protein levels, and LDH in PLF and BALF show that APMS-TEG are not inflammatory nor toxic when injected ($\sim 4 \times 10^7$ per mouse) intrapleurally in mice. Eosinophils and basophils in control PLF fluids at 3 d in both PBS control and APMS-TEG groups may reflect acute inflammation in response to injection of PBS, which has been reported in many instillation models. Mean ± SEM of individual experiments performed on a minimum of at least four mice/group/time point.

measured by LDH assays or observed by TEM. This lack of cytotoxicity may reflect the fact that APMS did not occur in membrane-bound phagosomes or merge with lysosomes. These processes are associated with cell uptake of foreign matter including toxic particulates such as asbestos fibers and silica particles (32, 33).

Although TEM and SEM images verified that APMS-TEG were taken up by MM cells, they also presented additional questions regarding mechanisms of uptake by cells. Flow cytometry studies showed that uptake at 4°C was not as efficient when compared with uptake of APMS-TEG at 37°C, reinforcing the premise that uptake of APMS-TEG is an active process in contrast to simple diffusion. We also incubated APMS-TEG with MM cells in the presence of filipin, a commonly used inhibitor of caveolae-mediated uptake, chlorpromazine, an inhibitor of receptor-mediated endocytosis and clathrin-mediated mechanisms, and cytochalasin D, known to disrupt actin filaments. Of these inhibitors, only pretreatment with cytochalasin D significantly inhibited the uptake of APMS-TEG by MM cells. These results indicate that the mechanisms of APMS-TEG uptake do not rely on clathrin or caveolae-mediated mechanisms, results contrary to studies in human melanoma cells where smaller particles (< 200 nm) enter cells via a mechanism involving clathrin-coated pits and larger particles (500 nm) are taken up via a caveolae-mediated mechanism (28, 34). No uptake of particles as large as 1 μm in diameter were observed in these studies (28, 34), an observation consistent with a number of studies showing that smaller particles are more easily taken up by a variety of cell types (35–37). In studies with fine and ultrafine (< 0.1 μM) titanium dioxide and polystyrene particles, particles were taken up into red blood cells and macrophages, and were not membrane-bound (37). Although cytochalasin D inhibited the uptake of 1 μM particles into cells, it did not affect uptake of smaller particles that was attributed to adhesive interactions and diffusion (37). The APMS used in our studies differ in that they are larger than ultrafine particles, are silica-based, and are coated with TEG, all factors potentially influencing their mechanisms of uptake by cells. Although the authors in the aforementioned study suggest that non–membrane-bound particles entering cells may have an enhanced toxicity due to their ability to directly

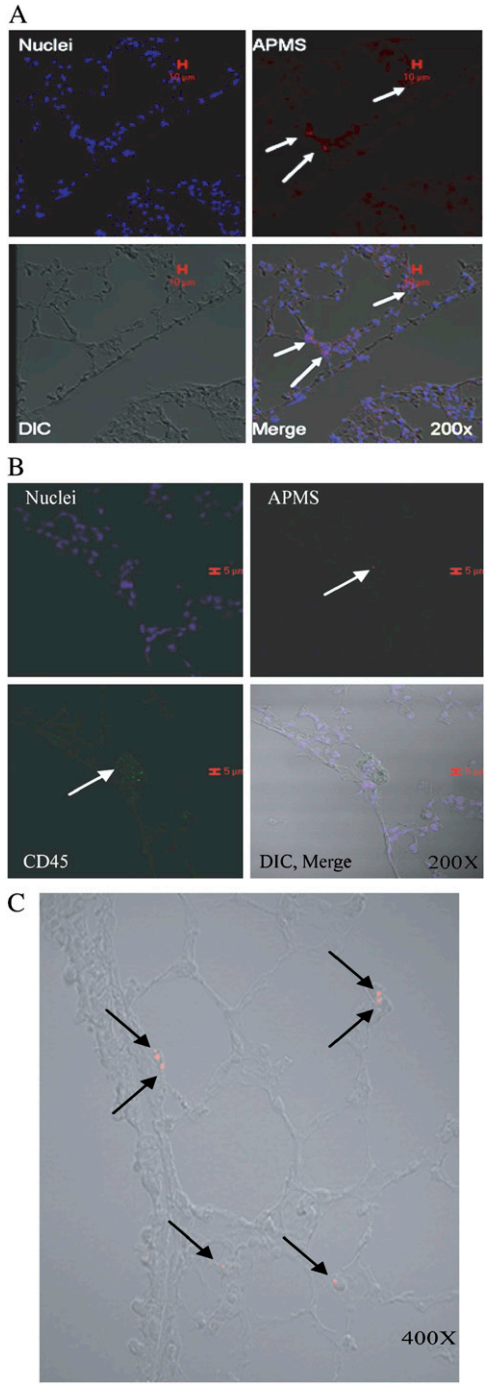

Figure 8. APMS-TEG are found in tissues after intrapleural injection and intranasal administration. After intrapleural injection, APMS labeled with Alexa 568 (*red*) were found in lung tissue after 3 d (A), and occasionally in CD45+ cells in the lung after 3 d (green) (B). Cell nuclei are indicated in blue (TOTO 3). When mice nasally inhaled APMS-TEG, APMS were found in cells of the lung at 24 h (C). In all experiments, $\sim 3.3 \times 10^7$ APMS were injected intrapleurally or inhaled intranasally. *Red scale bars* in *A* and *B* indicate 10 and 15 μm, respectively.

interact with intracellular proteins, organelles, and other macromolecules (37), APMS-coated particles were nontoxic to C10 and MM cells for extended periods of time (72 h). An advantage of using APMS as a vehicle to deliver constructs or anti-cancer drugs is that once inside a cell, the cargo carried by APMS would not be bound in vesicles or membranes and therefore would freely interact with intracellular target molecules for enhanced effects.

One of our objectives in modifying and studying intracellular trafficking of APMS is to develop their use in clinical studies, particularly for treatment of asbestos-associated MM. *In vivo* studies were undertaken to investigate whether APMS-TEG would be taken up by nearby cells when injected intrapleurally, mimicking topical exposure at sites of surgical debulking of tumors. Although some APMS-TEG were found in CD45+ leukocytes, most were found in other cell types in diaphragm and lung, indicating that APMS-TEG may be useful in delivering "cargo" such as chemotherapeutic drugs to cells adjacent to injection sites. In Figure 6, we present data indicating that APMS can be used as vehicles to carry DNA plasmids, which are then functionally expressed, inside of cells. Therefore, transfection of plasmids using APMS is possible, and studies are currently underway to increase its efficiency. Currently, we are investigating use of APMS with larger pores and with chemical modifications in pores that enhance the uptake and release of DNA.

We also wanted to determine whether administering APMS-TEG intrapleurally would lead to unwanted inflammation or cell damage after IP injection. As shown in Figure 7, APMS-TEG did not alter the normal cell profiles in BALF or PLF, nor cause increased protein or LDH activity. In addition, we explored the potential for APMS-TEG to be delivered to lungs of mice after intranasal inhalation. Using fluorescent APMS-TEG, we show that APMS-TEG enter alveolar septa in the peripheral lung tissue. These studies suggest that nebulization of APMS-TEG may be a possibility in treatment of early lung cancers or other airway diseases. At the time points tested (3 d and 7 d), APMS were neither toxic nor immunogenic. However, future studies will determine the long-term fate of APMS *in vivo*. These experiments will also reveal how long APMS persist, how they are eliminated from the body, and if they accumulate in other organs, as well as their possible chronic toxicity or immunogenicity.

Because APMS are $\sim$1–2 μm in diameter, considerably larger than nanoparticles, they are unlikely to penetrate the endothelial or blood–brain barrier and be carried systemically to other organs. Moreover, they cannot passively diffuse into cells and enter cell organelles, such as mitochondria or lysosomes, which may potentially disrupt normal cell respiration and cause cytotoxicity. Current studies also are underway to determine the utility of APMS-TEG as delivery devices for the chemotherapeutic drug, doxorubicin, in lung and pleural diseases (S. R. Blumen and coworkers, unpublished data).

Conflict of Interest Statement: S.R.B. does not have a financial relationship with a commercial entity that has an interest in the subject of this manuscript. K.C. does not have a financial relationship with a commercial entity that has an interest in the subject of this manuscript. M.E.R.-N. does not have a financial relationship with a commercial entity that has an interest in the subject of this manuscript. D.J.T. does not have a financial relationship with a commercial entity that has an interest in the subject of this manuscript. D.J.W. does not have a financial relationship with a commercial entity that has an interest in the subject of this manuscript. C.C.L. has patented APMS and is a founder of Apollo SR1 (a small company with an exclusive license to commercialize APMS). B.T.M. does not have a financial relationship with a commercial entity that has an interest in the subject of this manuscript.

Acknowledgments: The authors thank Trisha Barrett for her assistance with this manuscript; and Marilyn Wadsworth, Michele von Turkovich and Collette Charland for their excellent assistance obtaining confocal microscope images, SEM and TEM images, and with the flow cytometry studies, respectively.

References

1. Borm PJ, Kreyling W. Toxicological hazards of inhaled nanoparticles–potential implications for drug delivery. *J Nanosci Nanotechnol* 2004;4: 521–531.

2. Nel A, Xia T, Madler L, Li N. Toxic potential of materials at the nanolevel. *Science* 2006;311:622–627.
3. Oberdorster G, Oberdorster E, Oberdorster J. Nanotoxicology: an emerging discipline evolving from studies of ultrafine particles. *Environ Health Perspect* 2005;113:823–839.
4. United States Environmental Protection Agency. 2006. http://www.epa.gov/oar/particlepollution/fs20051220pm.html. Fact Sheet: Proposal to Revise the National Ambient Air Quality Standards for Particulate Matter.
5. Gallis KW, Araujo JT, Duff KJ, Moore JG, Landry CC. The use of mesoporous silica in chromatography. *Adv Mater* 1999;11:1452–1455.
6. Gallis KW, Landry CC. 2002. Mesoporous silica and method of making same. US Patent 6,334,988. USA.
7. Nassivera T, Eklund AG, Landry CC. Size-exclusion chromatography of low-molecular-mass polymers using mesoporous silica. *J Chromatogr A* 2002;973:97–101.
8. Guthrie GD, Mossman BT, editors. Health effects of mineral dusts, reviews in mineralogy. Washington, DC: Mineralogic Society of America; 1993.
9. Solberg SM, Landry CC. Adsorption of DNA into mesoporous silica. *J Phys Chem B Condens Matter Mater Surf Interfaces Biophys* 2006; 110:15261–15268.
10. Farokhzad OC, Cheng J, Teply BA, Sherifi I, Jon S, Kantoff PW, Richie JP, Langer R. Targeted nanoparticle-aptamer bioconjugates for cancer chemotherapy in vivo. *Proc Natl Acad Sci USA* 2006;103:6315–6320.
11. Maruyama K. PEG-immunoliposome. *Biosci Rep* 2002;22:251–266.
12. Olivier JC. Drug transport to brain with targeted nanoparticles. *NeuroRx* 2005;2:108–119.
13. Olivier JC, Huertas R, Lee HJ, Calon F, Pardridge WM. Synthesis of pegylated immunonanoparticles. *Pharm Res* 2002;19:1137–1143.
14. Martin-Herranz A, Ahmad A, Evans HM, Ewert K, Schulze U, Safinya CR. Surface functionalized cationic lipid-DNA complexes for gene delivery: PEGylated lamellar complexes exhibit distinct DNA-DNA interaction regimes. *Biophys J* 2004;86:1160–1168.
15. Huang M, Wu W, Qian J, Wan DJ, Wei XL, Zhu JH. Body distribution and in situ evading of phagocytic uptake by macrophages of long-circulating poly (ethylene glycol) cyanoacrylate-co-n-hexadecyl cyanoacrylate nanoparticles. *Acta Pharmacol Sin* 2005;26:1512–1518.
16. Sadzuka Y, Sugiyama I, Tsuruda T, Sonobe T. Characterization and cytotoxicity of mixed polyethyleneglycol modified liposomes containing doxorubicin. *Int J Pharm* 2006;312:83–89.
17. Hicke BJ, Stephens AW, Gould T, Chang YF, Lynott CK, Heil J, Borkowski S, Hilger CS, Cook G, Warren S, *et al.* Tumor targeting by an aptamer. *J Nucl Med* 2006;47:668–678.
18. Berna M, Dalzoppo D, Pasut G, Manunta M, Izzo L, Jones AT, Duncan R, Veronese FM. Novel monodisperse PEG-dendrons as new tools for targeted drug delivery: synthesis, characterization and cellular uptake. *Biomacromolecules* 2006;7:146–153.
19. Matsumura Y, Gotoh M, Muro K, Yamada Y, Shirao K, Shimada Y, Okuwa M, Matsumoto S, Miyata Y, Ohkura H, *et al.* Phase I and pharmacokinetic study of MCC-465, a doxorubicin (DXR) encapsulated in PEG immunoliposome, in patients with metastatic stomach cancer. *Ann Oncol* 2004;15:517–525.
20. Greenwald RB, Yang K, Zhao H, Conover CD, Lee S, Filpula D. Controlled release of proteins from their poly(ethylene glycol) conjugates: drug delivery systems employing 1,6-elimination. *Bioconjug Chem* 2003;14:395–403.
21. Greenwald RB, Choe YH, McGuire J, Conover CD. Effective drug delivery by PEGylated drug conjugates. *Adv Drug Deliv Rev* 2003;55: 217–250.
22. Greenwald RB, Conover CD, Choe YH. Poly(ethylene glycol) conjugated drugs and prodrugs: a comprehensive review. *Crit Rev Ther Drug Carrier Syst* 2000;17:101–161.
23. Malkinson AM, Dwyer-Nield LD, Rice PL, Dinsdale D. Mouse lung epithelial cell lines–tools for the study of differentiation and the neoplastic phenotype. *Toxicology* 1997;123:53–100.
24. Carpino LA. 1-Hydroxy-7-azabenzotriazole: an efficient peptide coupling additive. *J Am Chem Soc* 1993;115:4397–4398.
25. Schnitzer JE, Oh P, Pinney E, Allard J. Filipin-sensitive caveolae-mediated transport in endothelium: reduced transcytosis, scavenger endocytosis, and capillary permeability of select macromolecules. *J Cell Biol* 1994;127:1217–1232.
26. Wang LH, Rothberg KG, Anderson RG. Mis-assembly of clathrin lattices on endosomes reveals a regulatory switch for coated pit formation. *J Cell Biol* 1993;123:1107–1117.
27. Orlandi PA, Fishman PH. Filipin-dependent inhibition of cholera toxin: evidence for toxin internalization and activation through caveolae-like domains. *J Cell Biol* 1998;141:905–915.
28. Rejman J, Oberle V, Zuhorn IS, Hoekstra D. Size-dependent internalization of particles via the pathways of clathrin- and caveolae-mediated endocytosis. *Biochem J* 2004;377:159–169.
29. Tsakiridis T, Vranic M, Klip A. Disassembly of the actin network inhibits insulin-dependent stimulation of glucose transport and prevents recruitment of glucose transporters to the plasma membrane. *J Biol Chem* 1994;269:29934–29942.
30. Ramos-Nino ME, Vianale G, Sabo-Attwood T, Mutti L, Porta C, Heintz N, Mossman BT. Human mesothelioma cells exhibit tumor cell-specific differences in phosphatidylinositol 3-kinase/AKT activity that predict the efficacy of Onconase. *Mol Cancer Ther* 2005;4:835–842.
31. Altomare DA, You H, Xiao GH, Ramos-Nino ME, Skele KL, De Rienzo A, Jhanwar SC, Mossman BT, Kane AB, Testa JR. Human and mouse mesotheliomas exhibit elevated AKT/PKB activity, which can be targeted pharmacologically to inhibit tumor cell growth. *Oncogene* 2005; 24:6080–6089.
32. Mossman BT, Kessler JB, Ley BW, Craighead JE. Interaction of crocidolite asbestos with hamster respiratory mucosa in organ culture. *Lab Invest* 1977;36:131–139.
33. Persson HL. Iron-dependent lysosomal destabilization initiates silica-induced apoptosis in murine macrophages. *Toxicol Lett* 2005;159:124–133.
34. Wiewrodt R, Thomas AP, Cipelletti L, Christofidou-Solomidou M, Weitz DA, Feinstein SI, Schaffer D, Albelda SM, Koval M, Muzykantov VR. Size-dependent intracellular immunotargeting of therapeutic cargoes into endothelial cells. *Blood* 2002;99:912–922.
35. Prabha S, Zhou WZ, Panyam J, Labhasetwar V. Size-dependency of nanoparticle-mediated gene transfection: studies with fractionated nanoparticles. *Int J Pharm* 2002;244:105–115.
36. Desai MP, Labhasetwar V, Walter E, Levy RJ, Amidon GL. The mechanism of uptake of biodegradable microparticles in Caco-2 cells is size dependent. *Pharm Res* 1997;14:1568–1573.
37. Geiser M, Rothen-Rutishauser B, Kapp N, Schurch S, Kreyling W, Schulz H, Semmler M, Im Hof V, Heyder J, Gehr P. Ultrafine particles cross cellular membranes by nonphagocytic mechanisms in lungs and in cultured cells. *Environ Health Perspect* 2005;113:1555–1560.